Monte Carlo Simulation of Supported Metal Catalyst Sintering and Redispersion

Monte Carlo simulations of sintering and redispersion of supported metal catalysts, based on an atomic migration mechanism, are presented. The support surface was modeled as a square grid with metal atoms located at various grid points. Interaction energies between metal atoms, and between metal atoms and support sites were specified. The probability of movement of each metal atom during one time increment (iteration) was calculated from the interaction energies. The effects of interaction energies, metal loading and initial distribution of the metal were examined. The model predictions are in good qualitative agreement with experimental observations. The model predicts "apparent" movement, splitting and coalescence of entire metal particles; these experimentally observed phenomena have usually been cited as evidence that sintering occurs by a particle migration mechanism.

W. Glen Campbell, David T. Lynch, and Sieghard E. Wanke
Department of Chemical Engineering
University of Alberta
Edmonton, Alberta, Canada T6G 2G6

Introduction

Supported metal catalysts—catalysts which consist of metal dispersed over the surface of a support (carrier)—are an important class of industrial catalysts. One of the reasons for using supported metal catalysts rather than bulk metals, such as metal blacks and sponges, is the exceptional thermal stability of supported metal catalysts. Supported metal catalysts, such as Pt/γ-Al_2O_3, can be used at temperatures as high as 500°C for extended periods without significant loss in metal surface area, but the surface area of bulk metal powders, such as Pt black, decreases rapidly during exposure to temperatures as low as 150°C (Manninger, 1984). However, decreases in metal surface areas in supported metal catalysts do occur during prolonged use at elevated temperatures and during regeneration involving coke burn-off. The loss in metal surface area is due to an increase in the average size of the metal particles. The process by which this occurs is called sintering.

The results of numerous experimental studies of supported-metal-catalyst sintering have been reported during the last two decades, and several reviews have appeared on this subject (e.g., Wanke et al., 1987; Lee and Ruckenstein, 1983; Wanke and Flynn, 1975). Mathematical models have also been proposed for sintering. The early models were simple power law models which fit sintering data (metal surface area as a function of time) with a power law rate function (e.g., Hermann et al., 1961).

Correspondence concerning this paper should be addressed to S. E. Wanke.

The next generation of models were "phenomenological" models—models in which some general mechanistic steps were proposed for the overall sintering process. Ruckenstein and Pulvermacher (1973a,b) assumed that sintering occurred by migration of metal particles over the support surface followed by collision and coalescence of the migrating particles. This model will subsequently be referred to as the particle migration model. Flynn and Wanke (1974a,b) assumed that sintering occurred by detachment of metal atoms and/or metal-containing molecules from stationary metal particles, migration of these species over the support and capture of the migrating species by metal particles. This model will subsequently be referred to as the atomic migration model.

These two general mechanisms for sintering had previously been proposed by Mills et al. (1961), but it was not until a decade after Mills and his coworkers described these possible modes of sintering that mathematical formulations and predictions were done by Ruckenstein and Pulvermacher, and Flynn and Wanke. Experimental sintering results, in the form of metal surface area as a function of treatment time, cannot be used to differentiate between these two models since both models are able to describe the observed sintering behavior.

The reverse of sintering is redispersion, which is a process that increases the metal surface area by decreasing the average metal particle size. Much less information is available on redispersion, although redispersion is very important for the regeneration of sintered supported metal catalysts. The particle migration model cannot account for redispersion since average metal

particle sizes always increase according to this model. A particle-splitting mechanism was proposed by Ruckenstein and Pulvermacher (1973b) to overcome this deficiency of the particle migration model. The atomic migration model can account for redispersion by trapping migrating species at high energy sites on the support surface.

The inclusion of metal-support interactions is crucial for any redispersion model. Recent studies (e.g., Lietz et al., 1983; Foger and Jaeger, 1985) have clearly shown that the formation of metal-support complexes plays a key role in the stabilization and redispersion of supported metal catalysts. Previous models of sintering and redispersion have included energetic heterogeneities of the support surface, but these heterogeneities have usually been modeled as very strong "trap sites," i.e., metal species located on these sites are immobile (Rice and Chien, 1987). However, variations in the strengths of the metal-support interaction, which would incorporate reduced mobility of species located at the trap sites, and variations in the spatial distribution of the trap sites on the support surface have not previously been included in models. Another deficiency of most previous model predictions, including the recent Monte Carlo simulations by Handa and Matthews (1983) and Rice and Chien (1987), is that the location of the metal atoms and particles as a function of sintering time were not included in the simulation results. Knowledge about the location of metal particles as a function of time is crucial if the model predictions are to be used to discriminate between the atomic and particle migration models.

The prime objective for the work presented in this paper was to obtain predictions for a simple atomic migration model which included variations in metal-support interactions and provided the location of every metal atom as a function of time. The objective of the simulations was not to fit experimental sintering and redispersion data, but rather to determine whether the qualitative predictions of the model are in agreement with experimentally observed trends. The simulations showed that the simple atomic migration model is in agreement with the sintering and redispersion behavior of supported metal catalysts. The simulations showed that atomic migration can result in "apparent" movement and splitting of metal particles.

Model Description

The support surface was represented by a square grid of size $M \times M$, Figure 1a. Metal atoms, represented by the solid symbols in Figure 1a, could be situated at any of the (i, j) grid positions. However, only one atom was allowed to occupy a support position, i.e., a grid site could be empty or occupied by a single metal atom. Hence, it is a "two-dimensional" model, in which the metal atoms on the support surface were present as monolayer patches or as isolated metal atoms: i.e., the three-dimensional nature of metal particles is not included in the model. A three-dimensional model has to include the movements of metal species in and on the metal particles; inclusion of this feature in the model poses formidable computational problems which we have not yet solved. However, the two-dimensional model has all the qualitative features of a three-dimensional model, with the exception of metal particle shape and, hence, is a good starting point for detailed mechanistic modeling.

For the two-dimensional model, the location of each metal atom on the support grid is given by the coordinates (i, j) of the support grid on which the metal atom is located. The four grid locations $(i \pm 1, j)$ and $(i, j \pm 1)$ directly connected by grid lines

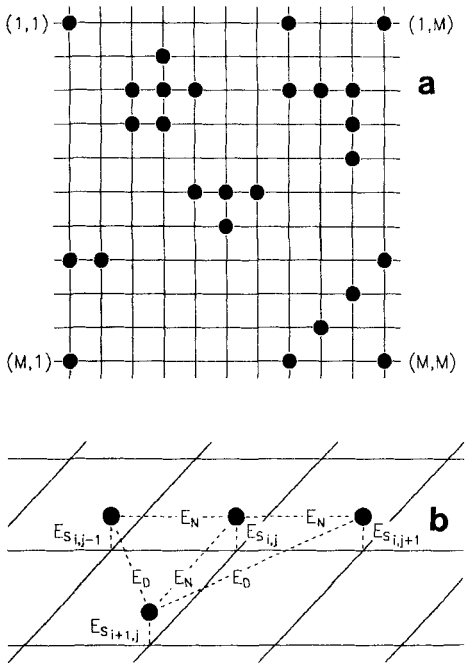

a) Metal particles on $M \times M$ grid
b) metal-metal and metal-support interaction energies.

Figure 1. Placement of atoms on two-dimensional grid.

to the occupied site (i, j) are called nearest-neighbor sites, while the four grid locations $(i \pm 1, j \pm 1)$ which are diagonal to site (i, j) are called diagonal-neighbor sites. The individual atoms are allowed to move only along the grid lines (to a nearest-neighbor site) and only provided that such a site is vacant: i.,e., the number of nearest-neighbor atoms for atom k, $N_{N,k}$, must be less than four in order for metal atom k to be able to move.

Despite the restriction on the direction of movement, a metal particle (an agglomeration of atoms) is considered to be composed of all the atoms which are connected to nearest- and diagonal-neighbor atoms. Thus, in Figure 1a there are particles containing six atoms in the upper-left region, four atoms in the central region, and five atoms in the upper-right region. The four diagonally situated atoms in the lower-right region are also considered to be part of a single particle; however, this particle actually contains seven atoms due to the treatment of the support-grid boundaries. The upper and lower boundaries, as well as the right and left boundaries, are assumed to be directly connected, so that the "two-dimensional" grid actually forms the surface of a torus. Thus, an atom can directly move from position (M, j) to position $(1, j)$ and vice versa, or from position (i, M) to $(i, 1)$ and vice versa. A consequence of this type of boundary connection is that the four atoms located at the corners of Figure 1a are actually members of a single particle of size four.

The energetics which govern the movement of atoms are shown in Figure 1b for the four-atom particle which is located in the central region of Figure 1a. Interaction energies, $E_{S_{i,j}}$, between metal atoms and support site (i, j) were assigned to each support site. This interaction energy between the support sites and the atoms can be different for every grid location. Atoms also have interaction energies E_N with nearest-neighbor atoms and E_D with diagonal-neighbor atoms. The values of these energies, E_D and E_N, are not functions of grid position. Thus, the

total interaction energy, $E_{i,j,k}$, of atom k, at location (i, j), with its neighboring atoms as well as with the support is given by:

$$E_{i,j,k} = E_{S_{i,j}} + N_{N,k}E_N + N_{D,k}E_D \quad (1)$$

where $N_{D,k}$ is the number of diagonal-neighbor atoms of atom k. All the energies used in this work are dimensionless quantities: the energies as defined are proportional to the bond energies divided by the absolute temperature.

The probability $P_{i,j,k}$ that atom k, at location (i, j), moves during one time interval (one iteration) is related to the total interaction energy via:

$$P_{i,j,k} = e^{-E_{i,j,k}} \quad (2)$$

Thus, $(1 - P_{i,j,k})$ is the probability of atom k not moving. It is assumed that each of the nearest-neighbor sites is an equally probable destination, regardless of whether other atoms are situated at these sites or not. The probabilities of moving to one of the four nearest-neighbor sites is $\frac{1}{4} P_{i,j,k}$. The possibility of movement to an occupied position is included in the initial probabilities since extension of the two-dimensional model to a three-dimensional model will require movement to occupied grid positions. The position of the atom after movement (or nonmovement) is determined from the product of five random numbers, $R(0, 1)$, with the five probabilities associated with the possible final states.

The maximum product fixes the destination. One of the following three situations can occur:

1. The atom does not move because $(1 - P_{i,j,k})R(0, 1)$ is the largest product.

2. The atom attempts to move away from location (i, j) because $(1 - P_{i,j,k})R(0, 1)$ is not the largest product, but the atom does not move because the intended new location is presently occupied by another atom.

3. Same as (2), except that the atom successfully moves because the intended location $(i \pm 1, j)$ or $(i, j \pm 1)$ is empty.

It should be noted that all of the atoms are not moved simultaneously, rather each of the N atoms on the grid is sequentially considered and moved if the calculations so indicate. However, for each iteration the order in which the atoms are considered is randomly adjusted, by making N random rearrangements of the numbers 1 to N, so that every atom has an equal chance of being moved first (or last).

Time does not appear explicitly in the calculations, but for a given simulation the number of iterations is directly proportional to time, where in one iteration the movement calculations are made for all of the N atoms on the grid. However, the time period per iteration for a fixed set of interaction energies is not fixed, since dimensionless interaction energies are used and the dimensionless interaction energies are proportional to the actual interaction energies divided by the temperature. The actual interaction energies depend on the nature of the metal species and the support. Hence, the time-equivalent of one iteration at a fixed set of dimensionless interaction energies depends on the temperature and the nature of the chemical species present. For example, the time period for one iteration for sintering of Pt in oxygen at 800°C is probably much less than 1 second, while one iteration may be equal to hours or days for sintering in hydrogen. It is possible to obtain estimates of the time period per iteration by comparing model prediction with experimental results (Rice and Chien, 1987). The objective of this paper, however, is to demonstrate that the two-dimensional model, based on an atomic migration mechanism, predicts the experimentally-observed trends for sintering and redispersion; it is not to fit experimental data.

The relative rates, at which sintering (or redispersion) occurs, depends on the $(E_N + E_D)$ to $E_{S_{i,j}}$ ratio. Large values of E_N (and E_D) relative to $E_{S_{i,j}}$, which can be due to strong metal-metal bonds and/or low temperature and weak metal support interactions, causes metal-metal bond cleavage to be rate controlling. This situation results in sintering. For large values of $E_{S_{i,j}}$, surface diffusion of isolated metal atoms is rate-controlling. Metal atoms that encounter sites with very large values of $E_{S_{i,j}}$ (trap sites) become localized, i.e., redispersion can occur.

The generation of random numbers is necessary for the atom movement calculations and for the randomization of the sequence in which individual atoms are examined. This was accomplished by using a random number generator of the linear congruential type in which uniform random numbers in the interval (0, 1), i.e., $R(0, 1)$ were generated by using:

$$R(0, 1)_{n+1} = [\{16{,}807R(0, 1)_n + 1\} \bmod (2^{31} - 1)]/(2^{31} - 1) \quad (3)$$

Details of this method for generation of random numbers are presented by Knuth (1981).

Inputs to Model

The objective of the simulations was to determine the effects of various parameters on the sintering and redispersion behavior predicted by the model. The parameters examined included the metal loading [the ratio of the number of metal atoms (N) to the number of grid sites (M^2)], the initial distribution of metal atoms on the support, the relative magnitudes of the metal-support and metal-metal interaction energies, and heterogeneity of the metal-support interaction energies. The influence of support grid size, at constant metal loading, was also investigated to determine conditions at which the predictions were independent of support grid size.

The following input parameters were specified for each simulation:

- Size of the $M \times M$ support grid.
- Number of metal atoms to be placed onto the support grid, N.
- Initial location of each metal atom on the support grid, (specification of i, j for each metal atom). The placements of the N metal atoms could be random, regular or predefined.
- Nearest-neighbor metal-metal interaction energy, E_N.
- Diagonal-neighbor metal-metal interaction energy, E_D. In all the simulations reported, $E_D/E_N = 0.5$ was used.
- Base metal-support interaction energy, $E_{s,b}$.
- Number of support sites, $N_{s,nb}$, which had interaction energies other than $E_{s,b}$.
- Metal-support interaction for nonbase support sites, $E_{s,nb}$. In all the simulations reported, a single value of $E_{s,nb}$ was used—the values of $E_{S_{i,j}}$ were either $E_{s,b}$ or $E_{s,nb}$.
- Grid locations of the $N_{s,nb}$ sites. The nonbase support sites were randomly distributed over the grid for the simulations presented in this paper.

The values of the input parameters for the various simulations are listed in Table 1. Some runs, such as 3, 3a, 3b and 3c, have the same input parameters, but the simulations were different since different initial random distributions and/or different random sequences for moving of atoms during the iterations were used.

Preliminary simulations were done to determine ranges of parameter values for which significant movement of atoms occurred in 50,000 to 100,000 interations. It was found that metal particles were very stable for $E_N + E_D$ greater than about 10: very little movement of atoms occurred. For $E_N + E_D$ less than about 1.5, metal particles were unstable and the concentration of single atoms on the support was high: very little sintering occurred. For $E_N + E_D$ values between 2 and 6, the results of the simulations were qualitatively similar except that more iterations were required to achieve the same degree of sintering or redispersion for the larger values of $E_N + E_D$; the general behavior was relatively independent of the E_D/E_N ratio. The rate of sintering was found to be approximately proportional to $e^{-(E_N+E_D)}$ for this range of interaction energies. Hence, values of $E_N = 2.0$ and $E_D = 0.5E_N$ where chosen for the base case (Runs 1 to 16, Table 1).

Table 1. Parameter Values and Initial Conditions for Simulations

Run No.	M	N	Init. Loc. of Metal Atoms	E_N	$E_{s,b}$	$N_{s,nb}$	$E_{s,nb}$	Total No. of Iterations
1	100	100	random	2	0	0		1.0×10^6
2	200	400	random	2	0	0		50,000
3	300	900	random	2	0	0		50,000
3a	300	900	random	2	0	0		75,000
3b	300	900	random	2	0	0		75,000
3c	300	900	random	2	0	0		75,000
4	400	1,600	random	2	0	0		1.0×10^7
4a	400	1,600	random	2	0	0		50,000
5	300	4,500	random	2	0	0		75,000
6	400	8,000	random	2	0	0		50,000
7	300	900	regular[1]	2	0	0		75,000
8	300	900	assigned[2]	2	0	0		75,000
9	300	900	assigned[3]	2	0	0		75,000
10	300	900	assigned[4]	2	0	0		75,000
11	300	900	assigned[5]	2	0	0		75,000
12	400	3,200	random	2	0	0		50,000
13	400	800	random	2	0	0		50,000
14	400	320	random	2	0	0		50,000
15	400	160	random	2	0	0		50,000
16	300	900	random[6]	2	0	0		75,000
17	100	100	random	2	0.5	0		75,000
18	100	100	random	2	1	0		75,000
19	100	100	random	2	2	0		75,000
20	300	900	assigned[3]	2	0	1,800	2	75,000
21	300	900	assigned[3]	2	0	1,800	6	75,000
22	300	900	assigned[3]	2	0	1,800	12	75,000
23	300	900	assigned[3]	2	0	450	12	75,000
24	300	900	assigned[3]	2	0	900	12	75,000
25	300	900	assigned[7]	2	0	1,800	6	300,000
26	300	900	assigned[8]	2	0	1,800	6	300,000
27	300	900	random	2	0	1,800	6	75,000
28	100	500	random	2	0	0		20,000

[1]Individual atoms with regular spacing on grid.
[2]100 9-atom particles evenly spaced on grid.
[3]36 25-atom particles evenly spaced on grid.
[4]25 36-atom particles evenly spaced on grid.
[5]20 9-atom particles and 20 36-atom particles evenly distributed on grid.
[6]Atoms placed randomly into central 134 × 134 square in center of 300 × 300 grid (this gives a local 5.0% metal loading).
[7]1 900-atom particle in center of grid.
[8]9 100-atom particles evenly spaced on grid.

Outputs of Simulations

The location of every metal atom on the support grid after every iteration was the primary output of the simulations. Graphical output of the location of metal atoms at specified iteration intervals was obtained. Typical results of this type of output are shown in Figure 2; the top panel in Figure 2 illustrates sintering behavior and the bottom panel illustrates redispersion. Location, size and shape of metal particles are given by this type of output, but its main use is the determination of changes in location of metal particle as a function of iteration number (treatment time). It is difficult (tedious) to obtain size distribution information from the graphical output. Hence, size distributions and average sizes of metal particles were calculated as part of the simulations.

Metal particle size distributions, in the form of number of metal particles as a function of number of metal atoms in the particles, were calculated at specified iteration numbers. Information about the average size of the metal particles was obtained from the average number of nearest neighbours, $N_{N,\text{avg}}$, and diagonal neighbours, $N_{D,\text{avg}}$ · $N_{N,\text{avg}}$ is defined as:

$$N_{N,\text{avg}} = \sum_{k=1}^{N} N_{N,k}/N \tag{4}$$

and $N_{D,\text{avg}}$ is given by:

$$N_{D,\text{avg}} = \sum_{k=1}^{N} N_{D,k}/N \tag{5}$$

The $N_{N,\text{avg}}$ and $N_{D,\text{avg}}$ values are related to the average size and shape of the metal particles, as will be discussed later.

Comments on Computation Times

All simulations, except Run 4, were done with an Amdahl 5870 computer. Simulations with the Amdahl required considerable CPU time; a typical simulation of 50,000 iterations for a 300 × 300 grid with 900 metal atoms (Run 3) required about 40 min of CPU time, while 50,000 iterations for a 400 × 400 grid with 8000 metal atoms (Run 6) required 340 min. Run 4 was done on a Cray XMP22 supercomputer, and the CPU time for the 10 million iterations for a 400 × 400 grid with 1600 atoms was 38 h. An equivalent run on the Amdahl would have required about 120 h of CPU time. Due to these rather large computing requirements, the number of iterations per simulation was usually kept to below 100,000.

Results and Discussion

The results for the various simulations described in Table 1 are presented in this section. The majority of the results will be presented as average metal particle size as a function of iteration number. Numerous average metal particle sizes have been defined (Anderson and Pratt, 1985), and all the average sizes can be calculated from the simulation results. However, in the current paper only averages based on the average number of neighbours will be used. For square metal particles, the average number of nearest-neighbors per metal atom in the particle, $N_{N,\text{sq}}$, is related to the number of metal atoms along the side of a

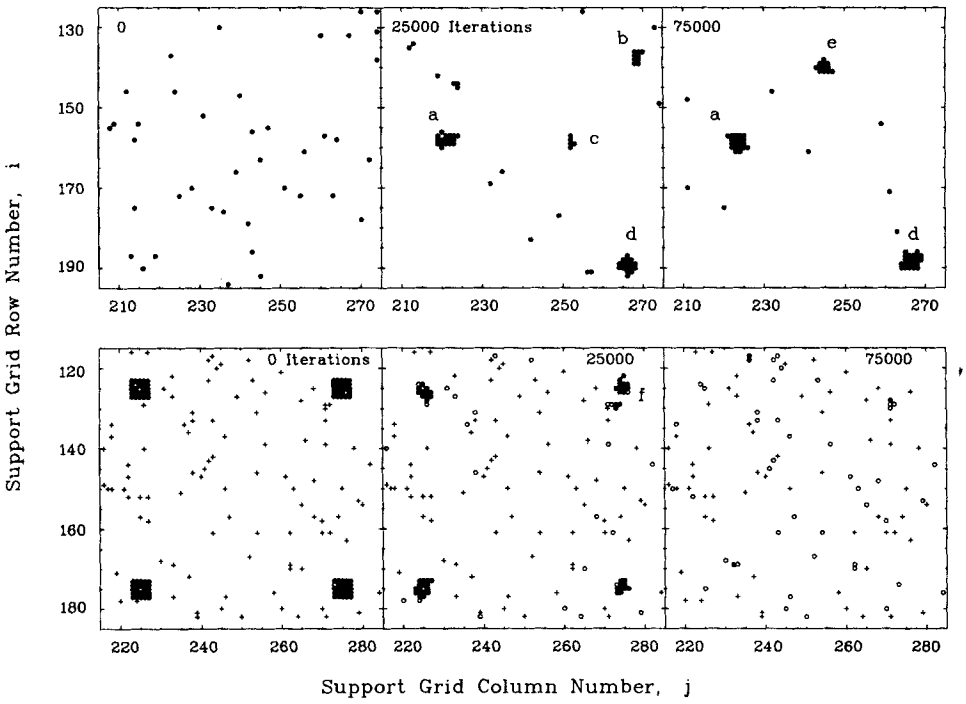

Figure 2. Typical graphical outputs from simulations.
Top—Run 3b; **bottom**—Run 21. ● = metal atoms on support site with base energy; O = metal atoms on support sites with nonbase energy; + = vacant nonbase energy site.

square particle, I_{sq}, by:

$$N_{N,sq} = 4[I_{sq} - 1]/I_{sq} \tag{6}$$

Hence, an equivalent average square-particle dimension, $I_{N,avg}$, is given by:

$$I_{N,avg} = 4/[4 - N_{N,avg}] \tag{7}$$

$I_{N,avg}$ is directly proportional to the average size of square particles. The value of $I_{N,avg}$, given by Eq. 7, is equal to the following average for a collection of square particles of different sizes:

$$I_{N,avg} = \Sigma n_{sq} I_{sq}^2 / \Sigma n_{sq} I_{sq} \tag{8}$$

An analogous average square particle dimension, $I_{D,avg}$, based on $N_{D,avg}$, is given by:

$$I_{D,avg} = 2/[2 - N_{D,avg}^{1/2}] \tag{9}$$

The two average particle dimensions, $I_{N,avg}$ and $I_{D,avg}$, would be equal if all metal particle were perfectly square; however, the shapes of the metal particles deviate considerably from being square, Figure 2. In subsequent plots, the average particle dimension defined by Eq. 9, i.e., $I_{D,avg}$, will be used.

The deviation from square shapes is also illustrated by the relationship between $N_{N,avg}$ and $N_{D,avg}$. For square particles, the relationship between the nearest and diagonal neighbors is

$$N_{D,avg} = N_{N,avg}^2/4 \tag{10}$$

However, the relationship between $N_{D,avg}$ and $N_{N,avg}$ obtained for sintering conditions with all support sites having $E_{S_{i,j}}$ equal to zero and a random initial distribution of atoms on the support was well described by

$$N_{D,avg} = N_{N,avg}^2/8 + N_{N,avg}/2 \tag{11}$$

These values of $N_{D,avg}$ are higher than those for square particles containing the same number of metal atoms. The significant deviations from the square shape result in values of particle dimensions which are lower than those that would be obtained by measuring the size of particles. However, the $I_{D,avg}$ values provide a good comparison of the effects of various parameters on the sintering and redispersion behavior.

Effect of Grid Size on Model Predictions

The size of the support grid used for the simulations should be sufficiently large so that the predictions are independent of the support grid size. Several simulations (Runs 1 to 5) were done to determine an appropriate grid size. The results of these simulations, Figure 3, show that the average metal particle sizes during the initial stages of sintering (<50,000 iterations) are relatively insensitive to grid size for values of M in the range of 100 to 400. During later stages of sintering significant fluctuations occurred for the 100 × 100 grid (open circles, Figure 3) because the number of large metal particles had decreased to one after about 500,000 iterations. Nevertheless, it was observed that the general trend for the 100 × 100 grid was the same as for the 400 × 400 grid even up to 1,000,000 iterations. To avoid the fluctuations in average particle size due to a small number of particles, 300 × 300 and 400 × 400 grids were used for most of the subsequent simulations.

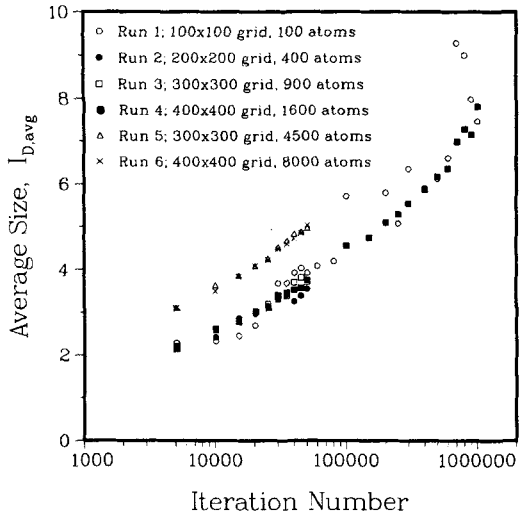

Figure 3. Effect of support grid size on sintering behavior.

Effect of Initial Conditions on Sintering Rates

The highly dispersed state of metal commonly present in fresh supported metal catalysts was simulated by randomly placing metal atoms onto support grid sites. Three cases with different initial random placements of 900 atoms on a 300 × 300 grid (Runs 3a, 3b and 3c) and one case in which 900 atoms were placed onto the grid with regular spacings (Run 7) were tested. The results of these four simulations, shown in Figure 4, demonstrate that the rate of sintering for these cases, for which the metal is initially well dispersed, is independent of the initial placement of metal atoms. Additional simulations showed that the sintering behavior was also not affected by altering the random sequence in which the atoms were moved in successive iterations. The metal particle size distributions as a function of iteration number are also relatively insensitive to the initial distribution for initially well-dispersed metal, Figure 5. The sizes of the individual metal particles were taken as the equivalent

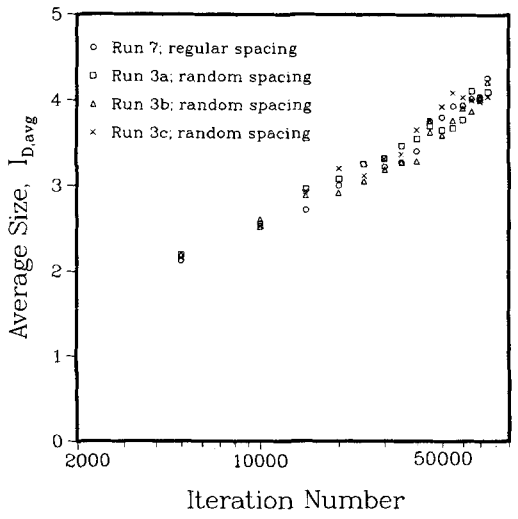

Figure 4. Effect of initial distribution of metal atoms on sintering behavior.

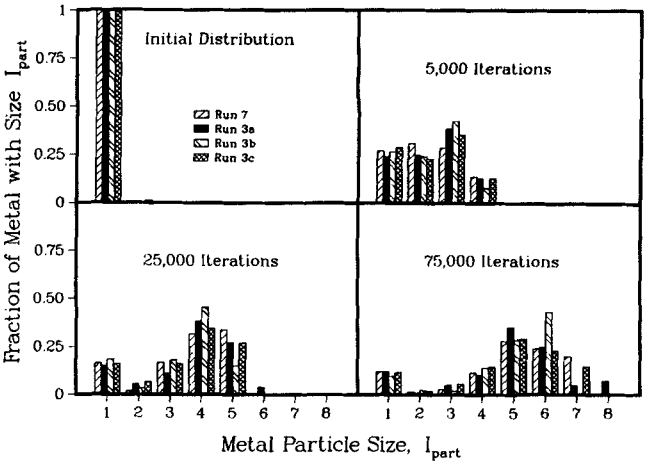

Figure 5. Metal particle size distributions as a function of initial distribution.

square particle size, i.e. the I_{part} was calculated as:

$$I_{part} = \sqrt{A_{part}} \tag{12}$$

where A_{part} is the number of metal atoms in a particle.

The results in Figures 4 and 5 are for the initial stages of sintering since the average particle size after 75,000 iterations was still small; the average of $I_{D,avg}$ for the four stimulations after 75,000 iterations was 4.16 (±0.10). One simulation, for a 400 × 400 grid containing 1,600 metal atoms (Run 4), was carried out for 10,000,000 iterations. The metal particle size distributions after selected numbers of iterations are shown in Figure 6. The following general observations can be made from these results:

1. The metal particle size distributions are narrow during the initial stages of sintering.
2. The size distributions become broader as sintering progresses.
3. There is a marked absence of small metal particles as sintering progresses (i.e., the distributions do not have a tail towards the lower sizes).

These general predictions of the model are in agreement with

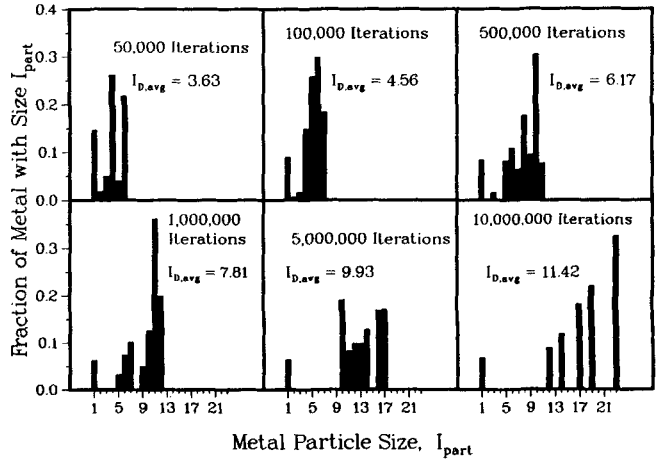

Figure 6. Metal particle size distributions as a function of number of iterations (Run 4).

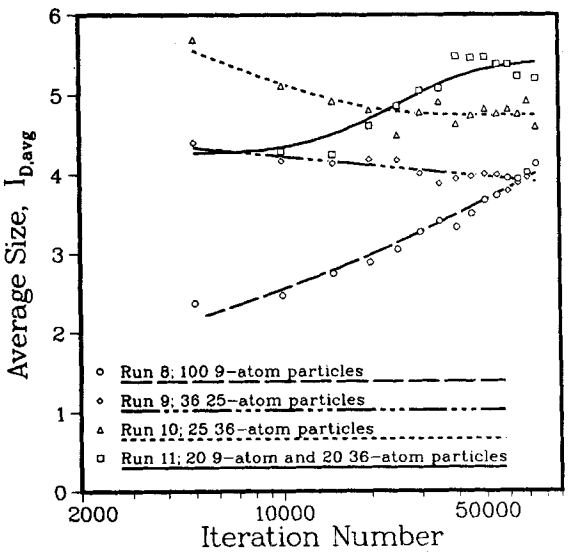

Figure 7. Effect of initial metal particle size on sintering behavior.

experimentally observed sintering behavior of $Pt/\gamma\text{-}Al_2O_3$ catalysts.

Sintering of $Pt/\gamma\text{-}Al_2O_3$ catalysts in He and H_2, even at 800°C, is slow, and the resulting Pt crystallite size distributions are relatively narrow (Guo et al., 1987). Sintering of $Pt/\gamma\text{-}Al_2O_3$ catalysts in O_2 at 700°C or higher is very rapid, and the Pt size distributions in heavily sintered catalysts are broad. Hence, this simple model predicts the observed trends for the sintering of $Pt/\gamma\text{-}Al_2O_3$ catalysts in inert, reducing and oxidizing atmospheres. The relationship between treatment time and number of iterations depends on the treatment atmosphere since the metal-metal interaction energies, E_N and E_D, are dependent on the atmosphere. E_N and E_D are much larger for inert and reducing atmospheres than for oxidizing atmospheres. Hence, one interation corresponds to a much longer treatment time in reducing atmospheres than in oxidizing atmospheres at constant treatment temperature.

The lack of a tail on the low-size side of the distribution is commonly cited as evidence that sintering of supported metal catalysts occurs via particle migration (Granqvist and Buhrman, 1976). The results in Figure 6 clearly show that atomic migration does not require such a tail in the distribution. A similar conclusion has previously been reached (Wanke, 1977). The size distributions shown in Figure 6 also do not support the use of a "time-invariant" generalized size distribution which is commonly used in models for sintering of supported metal catalysts (Ruckenstein and Pulvermacher, 1973a, b; Dadyburjor et al., 1986; Dadyburjor, 1987). Furthermore, the use of continuum diffusion models to describe the spatial variation of isolated metal atoms on the support surface (e.g., Dadyburjor et al., 1986) is very questionable since the concentration of isolated metal atoms is very low. In typical supported metal catalyst, less than 5% of the support surface is occupied by metal atoms, even if all the metal is present as isolated atoms (*vide infra*).

Several simulations were done to determine the influence of initial metal particle size and distribution on sintering behavior. The results for four of these simulations (Runs 8 to 11) are presented in Figures 7 and 8. The metal-support interaction energy for all four runs was zero, and a 300 × 300 grid with 900 atoms was used for all simulations. The initial distribution of the metal for these runs as follows:

Run 8: 100 square metal particles, each containing 9 metal atoms, were evenly distributed on the support grid.

Run 9: 36 square metal particles, each containing 25 metal atoms, were evenly distributed on the support grid.

Run 10: 25 square metal particles, each containing 36 metal atoms, were evenly distributed on the support grid.

Run 11: 20 square metal particles, each containing 9 metal atoms, and 20 square metal particles, each containing 36 metal atoms, were evenly distributed on the support grid. The spacing between the particles of different sizes was regular.

The results in Figure 7 show the variation in average metal particle size as a function of iteration number. The average

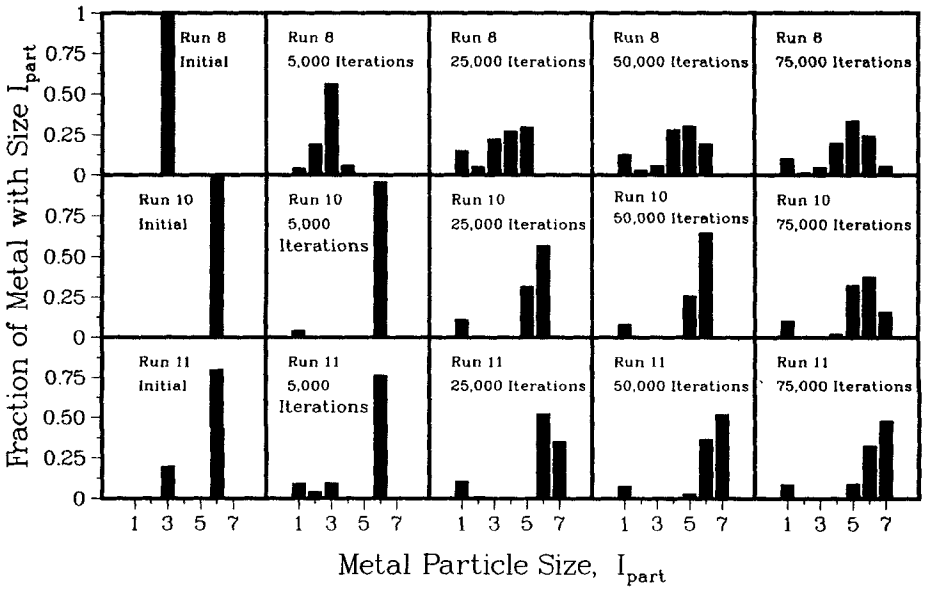

Figure 8. Effect of initial metal particle size on particle size distributions during sintering.

metal particle size decreases initially due to the formation of isolated metal atoms which dissociate from the particles and migrate over the support. It is evident, however, that the relative rate of sintering is the highest for the initially bimodal size distribution (Run 11). The higher rate of sintering for Run 11 is clearly demonstrated by the metal particle-size distributions shown in Figure 8. Other simulations showed that cases with broad or bimodal initial size distributions sintered more rapidly than cases with narrow initial size distributions. The dependence of sintering rate on initial metal particle size distribution predicted by the model cannot be compared with experimental observations since very little data on the effect of metal particle-size distribution on sintering rates is available.

Effect of Metal Loading on Sintering Rates

It is well established that increases in metal loading result in increased sintering rates. Typical metal contents for commercial Pt-group supported catalysts are in the 0.1 to 2 wt. % range, and support surface areas are usually 100 to 300 m^2/g of support. Hence, the fraction of the support surface occupied by metal atoms for well-dispersed catalysts varies from about 0.001 to 0.05. Simulations were done in which the metal loading, defined as the fraction of grid points occupied by metal atoms, was varied from 0.001 to 0.05 (Runs 4a, 6, 12 to 15). A 400 × 400 grid and values of zero for all metal-support interaction energies were used for these simulations. The initial state for these simulations was obtained by randomly placing the desired number of metal atoms onto the support grid. Variations in average metal particle size as a function of number of iterations and metal loading are plotted in Figure 9. These results are in agreement with the observation that sintering rates increase with increasing metal loadings. However, in many supported metal catalysts the metal is not evenly distributed over the support surface and regions on the support surface with local metal concentrations significantly greater than the average concentration may exist. This variations in spatial concentration should lead to increased sintering rates. The results for Run 16, in Figure 9, show that high local concentrations of the metal result in increased sintering rates.

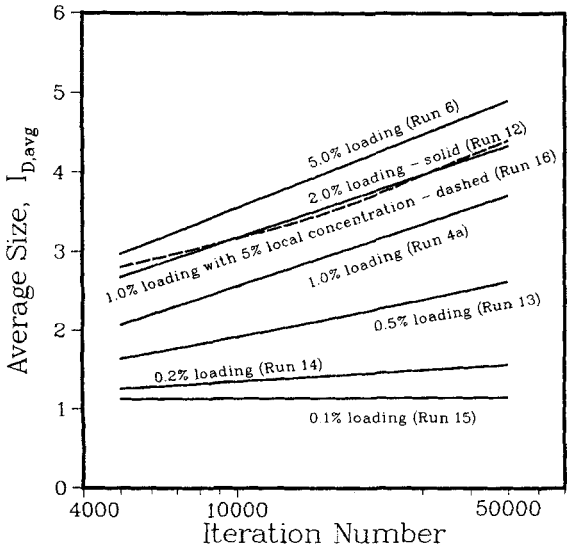

Figure 9. Effect of metal loading on sintering behavior.

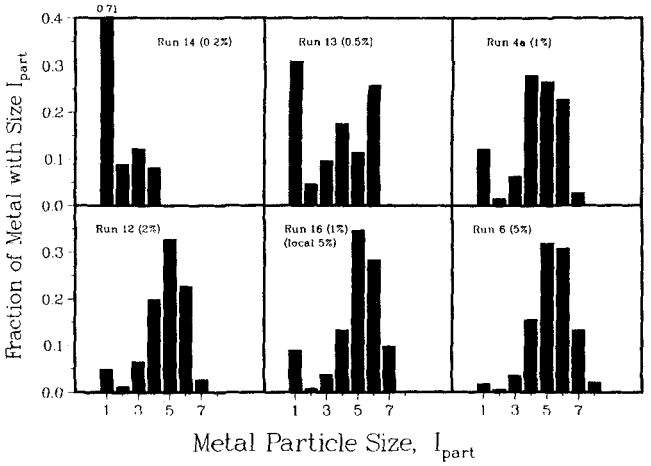

Figure 10. Metal particle size distributions after 50,000 iterations as a function of metal loading.

The average metal loading for Run 16 was 1.0%, but all the metal was initially located in a central region of the support occupying 20% of the total grid area, i.e., the effective local metal loading was 5%. The sintering behavior for Run 16 was very similar to the results for a 2.0% metal loading in which the metal was initially distributed over the total grid (cf., Runs 12 and 16 in Figure 9). Even the particle size distribution for Runs 12 and 16 were very similar as sintering progressed, Figure 10. The particle size distributions in Figure 10 show that the fraction of metal present as isolated atoms decreases with increasing metal loading.

Effect of Metal-Support Interactions on Sintering Rates

In all the previously discussed simulations, the metal-support interaction energies were set to zero. A value of zero for the metal-support interaction energy is probably a close approximation to sintering in inert and reducing atmospheres since nucleation studies by metal deposition from the vapor phase have shown that metal atoms are very mobile on supports under vacuum. However, for systems such as $Pt/\gamma\text{-}Al_2O_3$ in oxygen or chlorine containing atmospheres, the Pt forms complexes with the support surface and is rather immobile. Preliminary simulations with 100 × 100 grids containing 100 metal atoms (1% loading) were done to determine the effect the effect of $E_{s,b}$ on the sintering behavior. The results of these simulations, presented in Figure 11, show that sintering rates are very dependent on the magnitude of the $E_{s,b}/E_N$ ratio. Rapid sintering occurs for low values, while for $E_{s,b}/E_N = 1.0$ practically no sintering occurs for initially well-dispersed metal. Sintering of $Pt/\gamma\text{-}Al_2O_3$ in oxygen at temperatures below 600°C corresponds to high $E_{s,b}/E_N$ ratios, since no appreciable sintering of Pt occurs at these conditions.

Redispersion of Sintered Catalysts

Regeneration of sintered supported metal catalysts is commonly achieved by thermal treatments in chlorine-containing atmospheres (Wanke et al., 1987). The most likely mechanism for redispersion is the formation of localized metal—chlorine-support complexes. The formation of such complexes was simulated by assigning high metal-support interactions to selected grid locations (trap sites). These trap sites are referred to as nonbase support sites; the number of these nonbase energy sites is

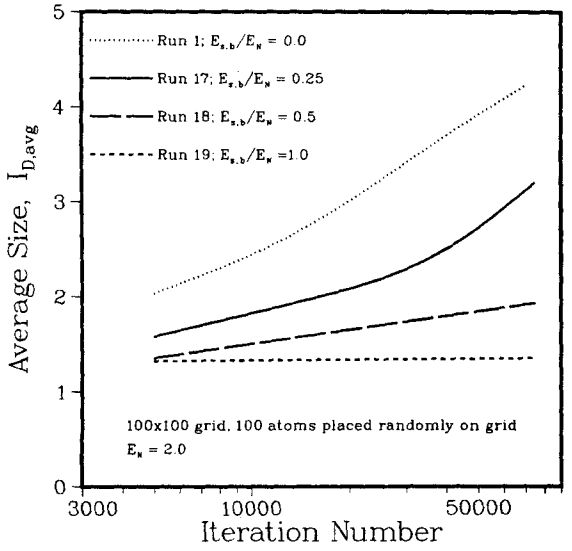

Figure 11. Effect of $E_{s,b}/E_N$ ratio on sintering behavior.

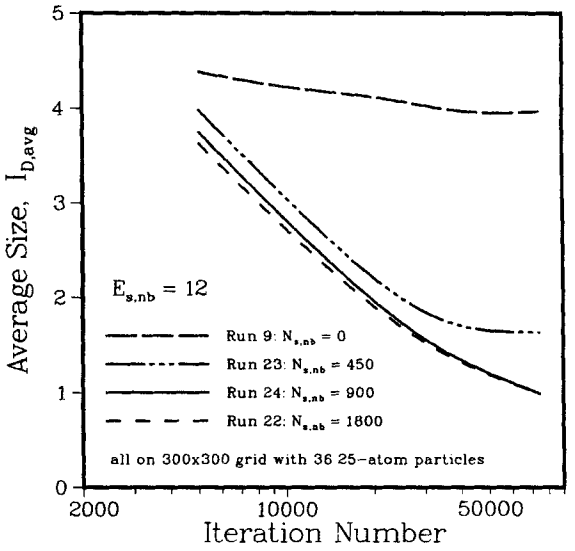

Figure 13. Effect of trap-site concentration on redispersion.

$N_{s,nb}$ and the metal-support interaction energy at these sites is $E_{s,nb}$. The influence of variations in $E_{s,nb}$, $N_{s,nb}$ and initial particle size on redispersion behavior was simulated.

The effects of changes in $E_{s,nb}$ at $N_{s,nb}$ = 1,800, E_N = 2.0 while keeping the initial metal particle size constant is shown in Figure 12. The effect of variations in $E_{s,nb}$ is very marked; at low values, redispersion is very slow (Runs 9 and 20). For $E_{s,nb}$ values equal to one-half of the total metal-metal interactions energy for a fully coordinated metal atom ($N_{N,k}$ = 4 and $N_{D,k}$ = 4) redispersion is rapid (Run 21), and further increases in $E_{s,nb}$ do not result in significant increases in redispersion rates (cf., Runs 21 and 22 in Figure 12).

The effect of variations in the concentration of trap sites ($N_{s,nb}$), with all other parameters held constant, is shown in Figure 13. If $N_{s,nb}$ is equal to or greater than the total number of metal atoms (N) and $E_{s,nb}/E_N$ is greater than about 3, then redispersion is rapid and essentially complete (Runs 22 and 24).

Note, if $N_{s,nb}$ is very large than redispersion would not occur because the metal particles would be anchored at trap sites. If $N_{s,nb}$ is less than N (Run 23), then redispersion is still rapid initially, but stops when most of the trap sites are occupied by metal atoms.

The effect of initial metal particle size, with all other parameters constant, is illustrated in Figure 14. It is well knwon that severely sintered catalysts are difficult to regenerate. The results in Figure 14 are in agreement with this observation. Complete redispersion of 25-atom particles is achieved in about 50,000 iterations (Run 21), while over 300,000 iterations are required for 100-atom particles (Run 26). For the 900-atom particle (Run 25) several million iterations would be required to achieve complete redispersion. (Note that the number of itera-

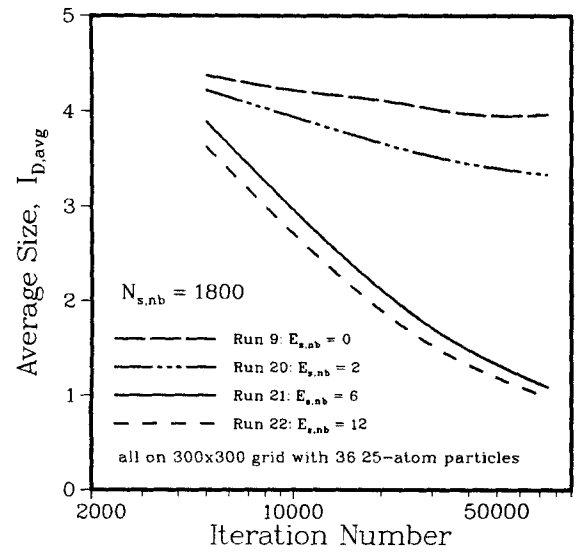

Figure 12. Effect of nonbase support interaction energy on redispersion.

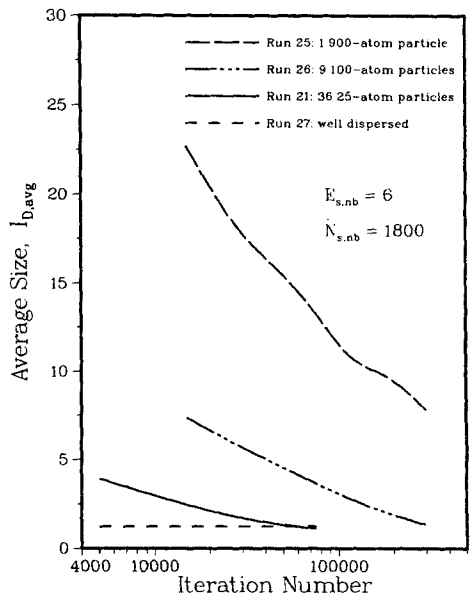

Figure 14. Effect of initial metal particle size on redispersion rates.

tions in Figure 14 are on a logarithmic scale.) Hence, the treatment times required for regeneration of heavily sintered catalysts, according to the predictions of the model, would very long (the number of iterations is proportional to the treatment time).

Location of Metal Particles on Support

The simulation results presented above are in agreement with the overall (macroscopic) sintering and redispersion behavior observed experimentally. In this section the microscopic (i.e., movement and location of metal atoms and particles) predicted by the model are compared with experimental observations. Same-area electron microscopic studies of model supported metal catalysts have been used to monitor the position of metal particles on supports as a function of treatment conditions. Chen and Ruckenstein (1981) describe several general events occurring during sintering of model Pd on γ-alumina samples. The general events observed include:

1. Disappearance of small metal particles and growth of large stationary particles.
2. Appearance of metal particles at previously vacant locations.
3. "Migration" of metal particles.
4. Contacting of metal particles with and without subsequent coalescence.
5. Formation of large faceted particles.

Chen and Ruckenstein (1981) discussed these observations in terms of particle migration and Ostwald ripening (atomic migration). All the observations above, except the formation of faceted particles, were observed in the graphical outputs from the simulations. The formation of faceted particles cannot be predicted by the two-dimensional model.

The disappearance of small particles and the growth of stationary large particles are illustrated in the top panels of Figure 2, i.e., between 25,000 and 75,000 iterations, Particle **c** disappeared and Particle **d** grew without moving appreciably. The appearance of a new particle at a previously vacant position is illustrated by Particle ***e***. This new particle resulted from collision and nucleation; it is not due to the migration of Particle ***b***. Particle ***a*** is an example of "apparent" particle migration. The particle has been displaced by several interatomic distances as a result of atom dissociation and capture. The symbol ***a*** in the top center and left panels is at the same grid location in the two figures. The apparent contacting and coalescence of metal particles is illustrated in Figure 15. In this figure sequences of what appear to be coalescence of particles, necking between particles and splitting of particles are illustrated. Examples of apparent particle splitting and size decreases during redispersion are shown in the bottom panels of Figure 2. Particles ***f*** resulted from the disintegration of the original 25-atom particle.

Hence, the atomic migration model can account for the observed events occurring during the sintering and redispersion of supported metal catalysts. It is not necessary to invoke the migration of entire metal particles to explain the observed phenomena.

Conclusions

The predictions of the simple atomic migration model described in this paper agree with the global changes in the state of the metal that have been observed as a result of sintering and redispersion of support metal catalysts. The qualitative effects of metal loading, metal particle size distribution and metal-support interaction energies are all well described by the model. The events observed in same-area electron microscopy studies, such as apparent movement and splitting of particles, are also predicted by the atomic migration model. To predict the formation of faceted particles requires a three-dimensional model. Computational methods, which significantly reduce computation time, have to be developed before attempting simulations for a three-dimensional model equivalent to the two-dimensional model analyzed in this paper.

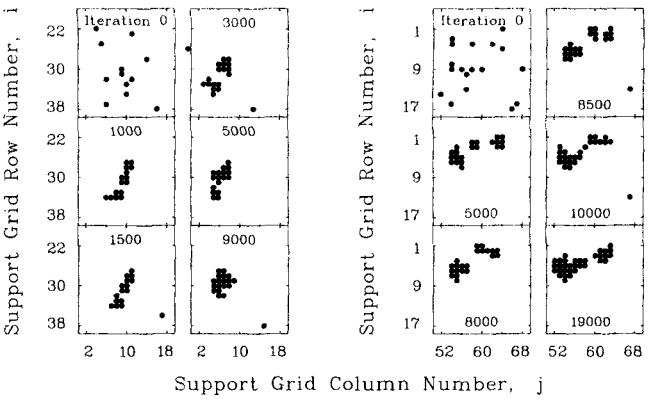

Figure 15. Apparent particle collision, coalescence and splitting (Run 28).

Acknowledgments

We gratefully acknowledge Computing Services at the University of Alberta for their special allocation of funds needed for the simulations with the Amdahl computer. We also thank Cray Canada Inc. for performing the simulation for Run 4 on the Cray supercomputer.

Notation

A_{part} = number of metal atoms in a particle
$E_{i,j,k}$ = total interaction energy between atom k at location (i,j) with the support site and the adjacent atoms
E_D = interaction energy between diagonal neighbor atoms
E_N = interaction energy between nearest-neighbor atoms
$E_{S_{i,j}}$ = support interaction energy at grid location (i,j)
$E_{s,b}$ = base value of support interaction energy
$E_{s,nb}$ = nonbase value of support interaction energy
$I_{D,avg}$ = average metal particle dimension based on $N_{D,avg}$ (equal to number of metal atoms alone one side of an equivalent square)
$I_{N,avg}$ = average metal particle dimension based on $N_{N,avg}$
I_{part} = equivalent dimension of square particle (equal to the square root of A_{part})
I_{sq} = number of metal atoms along one side of a square particle
M = size of the support grid
N = number of metal atoms on the support grid
$N_{D,avg}$ = average number of diagonal-neighbor atoms
$N_{D,k}$ = number of diagonal-neighbor atoms for atom k
$N_{N,avg}$ = average number of nearest-neighbor atoms
$N_{N,k}$ = number of nearest-neighbor atoms for atom k
$N_{N,sq}$ = average number of nearest-neighbor atoms in a square particle
$N_{s,nb}$ = number of support sites with nonbase interaction energy
n_{sq} = number of square particles of a given size
$P_{i,j,k}$ = probability of movement for atom at location (i,j)
$R(0,1)$ = uniform random number in the range (0,1)

Literature Cited

Anderson, J. R., and K. C. Pratt, "Introduction to Characterization and Testing of Catalysts," Ch. 2, Academic Press, New York (1985).

Chen, J. J, and E. Ruckenstein, "Sintering of Palladium on Alumina Model Catalysts in a Hydrogen Atmosphere," *J. Cat.*, **69**, 254 (1981).

Dadyburjor, D. B., "Multiparticle-Based Models for Sintering of Supported Metal Catalysts," *Catalyst Deactivation*, 21, B. Delmon and G.F. Froment, eds., Elsevier, Amsterdam (1987).

Dadyburjor, D. B., S. P. Marsh, and M. E. Glicksman, "The Role of Multiparticle-Adatom Interactions in the Sintering of Supported Metal Catalysts," *J. Cat.*, **99**, 358 (1986).

Flynn, P. C., and S. E. Wanke, "A Model of Supported Metal Catalyst Sintering: I. Development of Model," *J. Cat.*, **34**, 390 (1974a).

Flynn, P. C., and S. E. Wanke, "A Model of Supported Metal Catalyst Sintering: II. Application of Model," *J. Cat.*, **34**, 400 (1974b).

Foger, K., and H. Jaeger, "The Effect of Chlorine Treatments on the Dispersion of Platinum Metal Particles Supported on Silica and γ-Alumina," *J. Cat.*, **92**, 64 (1985).

Granqvist, C. G., and R. A. Buhrman, "Size Distributions for Supported Metal Catalysts Coalescence Growth versus Ostwald Ripening," *J. Cat.*, **42**, 477 (1976).

Guo, I., T.-T. Yu, and S. E. Wanke, "Changes in Pt Crystallite Sizes as a Result of Treating Pt/γ-Al_2O_3 Catalysts in Different Atmospheres," *Proc. North Amer. Cat. Soc. Mtg.*, J. Ward, ed., Elsevier, Amsterdam (in press).

Handa, P. K., and J. C. Matthews, "Modeling of Sintering and Redispersion of Supported Metal Catalysts," *AIChE J.*, **29**, 717 (1983).

Herrmann, R. A., S. F. Adler, M. S. Goldstein, and R. M. DeBaun, "The Kinetics of Sintering of Platinum Supported on Alumina," *J. Phys. Chem.*, **65**, 2189 (1961).

Knuth, D. E., "The Art of Computer Programming: Vol. 2, Seminumerical Algorithms," 2nd ed., Addison-Wesley, Reading, MA (1981).

Lee, H. H., and E. Ruckenstein, "Catalyst Sintering and Reactor Design," *Cat. Rev.—Sci. Eng.*, **25**, 475 (1983).

Lietz, G., H. Lieske, H. Spindler, W. Hanke, and J. Völter, "Reaction of Platinum in Oxygen- and Hydrogen-Treated Pt/γ-Al_2O_3 Catalysts," *J. Cat.*, **81**, 17 (1983).

Manninger, I., "The Kinetics of Pt-Black Catalyst Sintering in Different Atmospheres," *J. Cat.*, **89**, 164 (1984).

Mills, G. A., S. Weller, and E. B. Cornelius, "The State of Platinum in Reforming Catalysts," *Proc. Int. Cong. Cat.*, Paris, 2221 (1961).

Rice, R. W., and C. C. Chien, "Simulation of Supported Iridium Catalyst Sintering and Redispersion," *J. Cat.*, **103**, 140 (1987).

Ruckenstein, E., and B. Pulvermacher, "Kinetics of Crystallite Sintering During Heat Treatment of Supported Metal Catalysts," *AIChE J.*, **19**, 356 (1973a).

Ruckenstein, E., and B. Pulvermacher, "Growth Kinetics and Size Distributions of Supported Metal Crystallites," *J. Cat.*, **29**, 224 (1973b).

Wanke, S. E., "Comments on the Sintering Mechanism of Supported Metal Catalysts," *J. Cat.*, **46**, 234 (1977).

Wanke, S. E., and P. C. Flynn, "The Sintering of Supported Metal Catalysts," *Cat. Rev.—Sci. Eng.*, **12**, 93 (1975).

Wanke, S. E., J. A. Szymura, and T.-T. Yu, "The Sintering of Supported Metal Catalysts: Experimental Observations and Modeling," *Catalyst Deactivation*, E.E. Petersen and A. T. Bell, eds., Marcel Dekker, 65 (1987).

Manuscript received Oct. 21, 1987, and revision received Apr. 26, 1988.